From One-to-One to Many-to-Many: Dynamic Cross-Layer Injection for Deep Vision-Language Fusion

Cheng Chen[1*]   Yuyu Guo[1*]   Pengpeng Zeng[2]   Jingkuan Song[2]

Peng Di[1]   Hang Yu[1†]   Lianli Gao[†]

[1]Ant Group   [2]Tongji University

Abstract

*Vision-Language Models (VLMs) create a severe visual feature bottleneck by using a crude, asymmetric connection that links only the output of the vision encoder to the input of the large language model (LLM). This static architecture fundamentally limits the ability of LLMs to achieve comprehensive alignment with hierarchical visual knowledge, compromising their capacity to accurately integrate local details with global semantics into coherent reasoning. To resolve this, we introduce **Cross-Layer Injection (CLI)**, a novel and lightweight framework that forges a dynamic **"many-to-many"** bridge between the two modalities. CLI consists of two synergistic, parameter-efficient components: an **Adaptive Multi-Projection (AMP)** module that harmonizes features from diverse vision layers, and an **Adaptive Gating Fusion (AGF)** mechanism that empowers the LLM to selectively inject the most relevant visual information based on its real-time decoding context. We validate the effectiveness and versatility of CLI by integrating it into LLaVA-OneVision and LLaVA-1.5. Extensive experiments on 18 diverse benchmarks demonstrate significant performance improvements, establishing CLI as a scalable paradigm that unlocks deeper multimodal understanding by granting LLMs on-demand access to the full visual hierarchy.*

1. Introduction

Vision-Language Models (VLMs) [1–4] are increasingly viewed as a pivotal step toward Artificial General Intelligence. By endowing powerful Large Language Models (LLMs) with sight from Vision Transformers (ViTs) [5, 6], VLMs can perceive and reason about the world in a manner that more closely mirrors human cognition. Beneath this ambition, however, lies a profound architectural **symmetry** between ViTs and LLMs that most current designs shat-
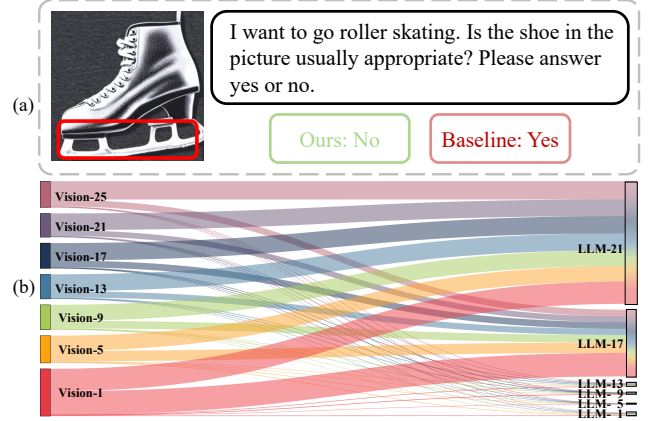

Figure 1. (a) An illustrative failure case where our baseline model, relying solely on final-layer features, incorrectly identifies an ice skate as 'roller skates'. This error underscores the necessity of accessing fine-grained details from early vision encoder layers. (b) Visualized gating weights from our CLI framework validate the efficacy of "criss-cross connections". The heatmap reveals that deeper LLM decoder layers (right) dynamically query features from the full spectrum of vision encoder layers (left)—a many-to-many interaction that confirms our proposed fusion architecture.

ter. Both are systems that progressively refine representations [7–9], yet they are connected by a crude, **asymmetric** bridge where only the top of the vision hierarchy is linked to the base of the language hierarchy. Such static and single-sided connection breaks the intrinsic hierarchical symmetry between ViTs and LLMs [7–9], leading to limited fine-grained perception and shallow multimodal reasoning.

This limitation has tangible consequences, as shown in Fig. 1 (a). A baseline VLM, relying only on final-layer features, recognizes the object as "roller skates" but overlooks critical wheel details, thus failing to assess its usability correctly. This failure highlights a fundamental **functional mismatch**: the static, single-layer connection denies the LLM access to the full spectrum of visual evidence, preventing it from integrating local details with global semantics for nuanced reasoning.

An effective integration must accommodate the diverse and dynamic needs of the LLM processing hierarchy. The

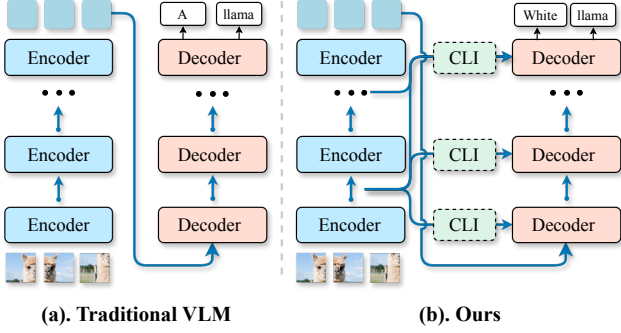arXiv:2601.10710v1 [cs.CV] 15 Jan 2026

1

Figure 2. (a) The Conventional VLM Pipeline. A vision encoder extracts features from its final layer, which are then mapped into the text embedding space by a projector. (b) Establishes a dynamic "many-to-many" bridge, extracting features from multiple vision layers and adaptively injecting them into multiple layers of the LLM.

most intuitive requirement is a parallel alignment: shallow LLM layers, processing local syntax [7], need access to early ViT layers capturing edges and textures [9] to ground basic nouns. Similarly, deep LLM layers handling abstract reasoning [8] would logically leverage high-level scene semantics from deep ViT layers [9]. Yet, even this parallel structure is still insufficient. The demands of sophisticated multimodal reasoning also necessitate **criss-crossed connections**. For instance, when processing the prompt in Fig. 1, a shallow LLM layer parsing the word "shoe" requires immediate access to the high-level, semantic concept of the object—an abstraction formed only in the deep ViT layers—to correctly ground the noun. Simultaneously, to answer the ultimate question, "Is the shoe...appropriate?", a deep LLM layer performing this evaluative reasoning must "zoom in" on the fine-grained structural details of the wheels—information captured only in the early ViT layers. This single example powerfully illustrates the need for both types of criss-crossed connections. Indeed, our own experiments confirm this necessity, revealing a complex pattern of learned connections (Fig. 1 (b)) that move far beyond a simple one-to-one mapping.

Solving this requires a fundamental shift from the prevailing one-to-one connections to a truly dynamic many-to-many framework. However, prior research attempting to bridge this gap offers only incomplete solutions: approaches like DeepStack [10] provide a form of brute-force one-to-many injection. Other models, from EVLM [11] to the recent Qwen3-VL [12], impose a heavyweight and rigid one-to-one fusion, hard-wiring specific vision layers to preconfigured LLM layers. All such methods create a static "straitjacket", failing to provide the dynamic, arbitrary access that sophisticated reasoning demands.

We argue that the solution is to empower the LLM to become an **active observer**, capable of dynamically querying the entire visual hierarchy at the precise level of de-

tail required by its current reasoning step. To this end, we are among the **first** to propose **Cross-Layer Injection (CLI)** (as shown in Fig. 2(b), a framework designed to realize a lightweight and adaptive **many-to-many** architecture for VLMs. CLI consists of two synergistic, parameter-efficient components. First, **Adaptive Multi-Projection** uses Low-Rank Adaptation (LoRA) [13] to efficiently harmonize features from diverse vision layers into a shared semantic space. Second, and most critically, our **Adaptive Gating Fusion** mechanism acts as an intelligent, context-sensitive controller. At each injection point, it allows the LLM to query this multi-level visual repository and selectively integrate only the most relevant information—be it fine-grained textures from a shallow ViT layer or abstract concepts from a deep one.

To validate the effectiveness and broad applicability of our CLI framework, we integrated it into two distinct VLM architectures: LLaVA-OneVision and LLaVA-1.5. Across 18 diverse and challenging benchmarks—covering key capabilities like document analysis, chart reasoning, and general visual perception—our method significantly outperforms the baseline models and other deep fusion strategies. In particular, when applied to LLaVA-OV-7B, our method achieves performance improvements of **6.5**, **3.3**, and **4.7** points on the LLaVA-in-the-Wild, MME, and the OCR-Bench benchmarks, respectively. To summarize, our main contributions are summarized as follows:

- A novel and lightweight framework, CLI, that systematically addresses the underutilization of hierarchical visual features in VLMs.
- Two synergistic and parameter-efficient modules, Adaptive Multi-Projection and Adaptive Gating Fusion, that collectively enable the alignment and dynamic, context-sensitive fusion of multi-level visual features.
- Extensive experiments on two distinct VLM architectures and a broad range of diverse benchmarks, demonstrating consistent and significant performance gains that establish a new state-of-the-art (SOTA) on several key tasks.

2. Related Works

2.1. The Dominant VLM Paradigm

The paradigm shift in AI driven by LLMs [14, 15] has naturally extended into the visual domain, leading to the rapid emergence of VLMs. A dominant architectural blueprint, established by seminal works like Flamingo [1] and BLIP-2 [2] and popularized by LLaVA [3, 4], is rooted in parameter-efficient adaptation. This approach involves freezing the powerful pre-trained vision and language backbones and training only a lightweight "bridge" module between them. This powerful and efficient design crystallized the "pre-training + fine-tuning" paradigm that now dominates the field, sparking a wave of open-source innovation, includ-

ing InstructBLIP [16], MiniGPT-4 [17, 18], Qwen-VL [19], and InternVL-2.5 [20]. Beneath this success, however, lies the fundamental architectural flaw we identify in our introduction: these models almost universally treat the output of the final vision encoder layer as the sole representation of the image, creating a severe information bottleneck and limiting the LLM's perceptual depth.

2.2. Deeper Fusion: Hierarchical Approaches

To address the above problem, subsequent research has explored deeper visual-language fusion strategies.

One-to-Many Injection: Brute-Force and Context-Blind. The first category attempts to inject features from a single image (one) into multiple LLM layers (many) through direct, non-adaptive methods. DeepStack [10] is a prominent example of this approach, partitioning high-resolution visual tokens and injecting them into different LLM layers via simple element-wise addition. This brute-force mechanism is context-blind; the non-adaptive summation risks disrupting the LLM's carefully learned representations by injecting unfiltered, and potentially irrelevant, visual information. Other work, such as FUSION [21], deepens the fusion process by introducing "interaction layers" where learnable tokens recursively engage with both textual and visual features. However, this approach focuses on the recursive interaction self and still operates on a single level of visual representation.

Statically-Wired One-to-One Fusion: Rigid and Inflexible. The second category employs dedicated modules to create fixed connections between specific vision and LLM layers, forming a kind of one-to-one mapping at different points in the hierarchy. Flamingo-style architectures like EVLM [11] exemplify this by inserting a new cross-attention layer before each LLM layer and feeding it features from a specific, pre-assigned ViT layer. This philosophy of sparsely inserting specialized fusion blocks into a pre-configured structure is also seen in models like mPLUG-Owl3 [22], which places "Hyper Attention" blocks at predetermined layers to run cross-attention. More recent models like Qwen3-VL [12] similarly rely on a pre-determined, hard-wired connection scheme. All these approaches lock the model into a manually configured, static "straitjacket" that predetermines a fixed information flow, preventing the LLM from dynamically accessing visual information based on its real-time reasoning needs.

Our CLI framework aims to overcome the limitations of the aforementioned methods. Unlike the context-blind addition of DeepStack, our Adaptive Gating Fusion ensures information is integrated selectively and precisely. Unlike the rigid, hard-wired architectures of EVLM and mPLUG-Owl3, our framework provides lightweight, on-demand access to the entire visual hierarchy at every injection point, finally enabling the stable and dynamic many-to-many fu-

sion that sophisticated multimodal reasoning requires.

3. Method

This section details the Cross-Layer Injection (CLI) framework. By replacing the conventional crude connections with a dynamic **many-to-many** bridge, CLI overcomes the information bottleneck that perceptually impoverishes VLMs. We first review the standard VLM pipeline in Sec. 3.1 to contextualize its limitations. Subsequently, Sec. 3.2 details the proposed mechanism. As shown in Fig. 3, it consists of two core components. The first component is **Adaptive Multi-Projection (AMP)**, a parameter-efficient module that uses LoRA to align multi-level visual features with the language space. The second, **Adaptive Gating Fusion (AGF)**, is a query-based attention gate that dynamically integrates these aligned features into the LLM's hidden state during the decoding process.

3.1. Preliminaries

The traditional VLM architecture (see Fig. 2(a)) comprises a visual encoder, a projector, and an LLM. First, the visual encoder extracts features from an input image I:

$$V = \text{ImageEncoder}(I), \quad V \in \mathbb{R}^{N_i \times D_i}, \quad (1)$$

where V consists of N_i visual tokens, each with a dimension of D_i. A projector module P, typically an MLP, then aligns these visual tokens with the language embedding space:

$$\hat{V} = P(V) = \text{MLP}(V), \quad \hat{V} \in \mathbb{R}^{N_i \times D_t}, \quad (2)$$

where the output dimension D_t matches the dimension of the text tokens. Simultaneously, the input text, $Text$, containing user instructions and prompts, is embedded into a sequence of N_t text tokens. The projected visual tokens $\hat{V}$ and the text tokens T are concatenated to form a unified multimodal context, $\mathbf{H} = [\hat{V}; T]$, on which the LLM performs auto-regressive decoding:

$$P(w_{t+1}|w_{1:t}, \mathbf{H}) = \text{LLM}(w_{1:t}, \mathbf{H}). \quad (3)$$

This dominant paradigm's critical flaw, as argued in our introduction, is its reliance on only the final-layer visual features. This rigid one-to-one connection creates a severe information bottleneck by discarding the rich hierarchical information captured in earlier ViT layers.

3.2. Many-to-Many Cross-Layer Injection

To overcome this fundamental limitation, we introduce Many-to-Many Cross-Layer Injection, a framework that restores this symmetry by forging a dynamic many-to-many bridge between the vision encoder and the LLM decoder, as shown in Fig. 3. Instead of a single point of contact, our approach empowers the LLM to dynamically access and integrate multi-level visual features at various stages of its own decoding process, conditioning its reasoning on a far more comprehensive visual context.
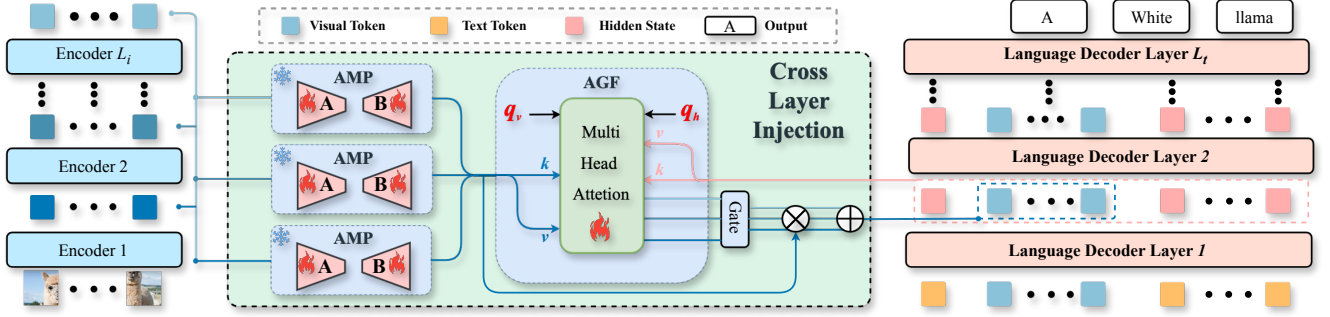
Figure 3. An overview of the proposed Cross-Layer Injection (CLI) Framework. The left panel illustrates the overall "many-to-many" information flow, where hierarchical features from multiple vision encoder layers are dynamically injected into the LLM at multiple decoder layers. The right panel details the core **Adaptive Gating Fusion** module that enables this process. Multi-Head Attention (MHA) first distills key information from both the incoming visual features and the current LLM hidden state. A gate controller then uses these distilled representations to compute a dynamic weight that governs the selective fusion of the new visual information. This gated process ensures the feature injection is both adaptive and context-sensitive, preventing the LLM from being overwhelmed by irrelevant data.

Our method begins by extracting a hierarchical set of visual features. Instead of using only the final layer, we sample intermediate token matrices from L_i distinct layers of the vision encoder, forming a collection $\mathbb{V} = \{V_l\}_{l=1}^{L_i}$. This strategy ensures that the model can access both low-level structural features from early layers and high-level semantic concepts from later ones. For instance, sampling from layers 1, 7, and 14 would produce the feature set $\mathbb{V} = \{V_1, V_7, V_{14}\}$. To integrate these multi-level features during reasoning, we introduce cross-layer injection points at multiple layers within the LLM's decoder. This is operationalized through our novel **AMP** and **AGF**. At a specific layer in the LLM, these modules take the entire set of hierarchical visual features $\mathbb{V}$ as input, aggregate this information, and inject a synthesized representation. This allows the LLM to dynamically condition its output on the most relevant visual details, regardless of their layer of origin.

Adaptive Multi Projection (AMP). A central component of our mechanism is a specialized projection module designed to align multi-level visual features with the language embedding space. Aligning multi-level visual features presents a fundamental projection dilemma. On one hand, a single, rigid projector cannot reconcile the significant distributional variance across vision layers—from low-level textures to high-level semantics—leading to severe feature misalignment. On the other hand, the seemingly obvious alternative of training a dedicated projector for each layer is computationally prohibitive due to the extensive pretraining required. Therefore, our solution is to make the projector *adaptive* in a parameter-efficient manner. We employ LoRA to modify the behavior of the original, pre-trained projector. Specifically, for the visual tokens $V_k \in \mathbb{V}$ drawn from a sampled layer k, we augment the pre-trained MLP within the projector with a unique, layer-specific LoRA projector. This adaptive projection is:

$$\hat{V}_k = P(V_k) + \text{LoRA}(V_k) \quad (4)$$

$$= \text{MLP}(V_k) + B_k A_k(V_k), \quad V_k \in \mathbb{V}, \quad (5)$$

where A_k and B_k are the low-rank matrices trained specifically for features from vision layer k. This adaptive projection process is applied to each feature map $V_k \in \mathbb{V}$, yielding a new set of aligned token maps $\hat{\mathbb{V}} = \{\hat{V}_k\}_{k=1}^{K}$. Each component $\hat{V}_k$ within this set is now harmonized in the text embedding dimension, making the entire hierarchical collection ready for effective integration into the LLM.

Adaptive Gating Fusion (AGF). With the visual tokens aligned, the next step is their effective integration. Rather than using a simple summation, which can disrupt the LLM's state, we propose an adaptive injection mechanism. This approach acknowledges that the LLM's hidden state, h, already contains contextual information and thus requires a more nuanced update. Accordingly, for each injection layer L_t in the LLM, a gating module is proposed to dynamically assess the relevance of the new visual features, $\hat{V}_k \in \hat{\mathbb{V}}$, based on the current decoding context h_t. The gate's logic is driven by cross-attention. Two learnable query vectors, q_v and q_h, act as probes to distill the essence of the new visual information and the existing hidden state:

$$\hat{V}_{\text{att}} = \text{MultiHeadAttention}(q_v, \hat{V}_k, \hat{V}_k), \quad (6)$$

$$h_{\text{att}} = \text{MultiHeadAttention}(q_h, h_t, h_t). \quad (7)$$

The resulting context vectors are fused and passed through a gate controller—a linear layer followed by a Sigmoid activation—to yield a dynamic weight, $W \in [0, 1]$:

$$W = \text{Sigmoid}(\text{Gate}([\hat{V}_{\text{att}}; h_{\text{att}}])). \quad (8)$$

This weight governs the selective update of the hidden state. To ensure precision, we use a binary "mask" that isolates the positions of visual tokens within h_t. The non-visual portions are preserved, while the visual portions are updated via a weighted sum with the new features:

$$h'_t = h_t \odot (1 - \text{mask}) + (h_t \odot \text{mask} + W \odot \hat{V}), \quad (9)$$

where $\odot$ denotes element-wise product. This fusion process enriches the hidden state h_t with a hierarchical representa-

tion of the visual input through processing all the $\hat{V}_k$ in $\hat{\mathbb{V}}$. This gating and update cycle is repeated at designated injection points throughout the LLM's decoder. This method facilitates an iterative refinement of the model's visual understanding, allowing it to "re-examine" visual evidence at varying granularities throughout the generation process.

4. Experiments

This section presents a comprehensive empirical validation of our Cross-Layer Injection (CLI) framework. We first detail the experimental setup, including our implementation of CLI on two distinct VLM architectures and the benchmarks used for evaluation. Then, the main results are presented, demonstrating that CLI consistently and significantly outperforms strong baselines and competing fusion strategies across 18 diverse benchmarks. Finally, a series of in-depth ablation studies and analyses are conducted to dissect the specific contributions of CLI's core components and validate our "many-to-many" design philosophy.

4.1. Experiment Setup.

Model Configuration. To demonstrate the versatility and general applicability of CLI, we integrate it into two distinct VLM architectures, LLaVA-OneVision [23] and LLaVA-1.5 [4]. The specific components for each are as follows:
- **CLI on LLaVA-OneVision**: This model uses a Qwen-2 series model [24] as the LLM backbone, a Siglip-so400m-patch14-384 [6] vision encoder, and a two-layer MLP projector. To mitigate potential data contamination and ensure a fair evaluation, we initialize our fine-tuning from the public checkpoint released after its "High-Quality Knowledge Learning" stage.
- **CLI on LLaVA-1.5**: This variant is built upon Vicuna-7B [25] as the LLM and CLIP-Large [5] as the vision encoder, with a two-layer MLP projector using a GELU activation. Following the methodology of LLaVA-1.5, we fine-tune the model starting from the pre-trained checkpoint and using the identical training data.

We adopt the original training protocols from LLaVA-OneVision and LLaVA-1.5. Detailed hyper-parameters for our experiments are listed in Appendix A.

Dataset Configuration. The foundation of our instruction tuning set consists of the single-image datasets from LLaVA-OneVision, which provide a broad base for general visual understanding (see Appendix B for details).

Evaluation Benchmarks. To ensure a standardized and reproducible comparison, we evaluate the LLaVA-OneVision and LLaVA-1.5 models across a comprehensive suite of single-image benchmarks using the LMMs-Eval framework [26]. These benchmarks are grouped into three primary categories to assess a wide range of capabilities (details can be found at Appendix C):

- **Chart, Diagram, and Document Understanding**: AI2D [27], ChartQA [28], DocVQA [29], and InfoVQA [30]. These tasks demand fine-grained perception of text and structural elements.
- **Perception and Multidisciplinary Reasoning**: MME [31], MMBench [32], MMVet [33], MathVerse [34], MathVista [35], MMMU [36], GQA [37], OK-VQA [38], ScienceQA [39], SEED-Bench [40], MM-Star [41], and POPE [42]. These benchmarks test abstract reasoning, knowledge integration, and resistance to hallucination.
- **Real-world Understanding and Visual Chat**: RealworldQA [43], LLaVA-in-the-Wild [4]. These qualitative benchmarks evaluate the model's practical conversational and reasoning abilities in open-ended scenarios.

Comparison Methods. We evaluate our method against two sets of competitors. First, to situate our model's performance in the broader landscape, we compare it against SOTA VLMs at both similar (IXC-2.5-7B [44], InternVL-2-8B [45]) and larger scales (VILA-13B [46], InternVL-2-26B [45]). Additionally, to directly assess our fusion strategy, we conduct a controlled study comparing CLI against three fusion paradigms, all implemented on the same base models and trained on the identical dataset. Our primary comparison is against the **Baseline Projector**, the original single-layer projection method from the LLaVA architecture, which we re-trained to serve as a fair baseline (referred to as LLaVA-OV-0.5B/7B). We also compare against **DeepStack** [10], a brute-force one-to-many approach that injects only final-layer visual tokens into multiple LLM layers, and **Shallow-Layer Injection (SLI)**, a rigid statically-wired method used by models like Qwen3-VL [12] that creates a fixed one-to-one mapping from the first n vision layers to the corresponding initial n LLM decoder layers.

4.2. Main Results

We evaluate our CLI by incorporating them into LLaVA-OneVision and LLaVA-1.5 architectures. Quantitative results compared with SOTA methods and other fusion works are shown in Tabs. 1 and 2. Overall, these results show that our CLI framework significantly outperforms the Baseline Projector (labeled LLaVA-OV-0.5B and -7B) across both model scales. This validates our central hypothesis: empowering an LLM with dynamic, on-demand access to the full visual hierarchy unlocks a deeper level of multimodal understanding. Furthermore, the performance lift from CLI is substantially larger than that of other deep fusion strategies, and it is the only method to deliver robust gains over the baseline. DeepStack, with its context-blind addition, often degrades performance, falling well below the baseline and demonstrating that unfiltered feature injection is disruptive. Shallow-Layer Injection delivers only marginal or inconsistent gains, failing to significantly improve upon the baseline because it confines multi-level visual data to

Table 1. Performance evaluation of the proposed CLI framework across a suite of nine benchmarks. We integrate our proposed Cross-Layer Injection (CLI) framework into LLaVA-OV (0.5B, 7B) and compare against baselines and alternative fusion methods. The table shows that CLI consistently provides significant performance gains over the baselines and substantially outperforms competing fusion methods, especially on complex reasoning tasks like LLaVA-in-the-Wild.

Model	AI2D	ChartQA	DocVQA	InfoVQA	RealWorldQA	LLaVA-W	POPE	OK-VQA	GQA	Sum
	test	test	val	val	test	test	test	val	test	
VILA-13B [46]	57.6	32.8	20.0	10.0	41.9	58.6	0.4	1.6	17.6	240.5
IXC-2.5-7B [44]	39.1	81.2	90.3	68.1	57.5	63.2	88.5	29.2	57.7	574.8
InternVL-2-8B [45]	82.2	82.5	90.0	66.5	64.4	72.7	87.8	52.1	62.7	660.9
InternVL-2-26B [45]	83.0	84.4	90.4	68.9	67.2	90.6	88.8	48.3	65.1	686.7
LLaVA-OV-0.5B	56.5	64.5	64.1	**47.5**	56.0	**61.7**	88.8	48.4	53.7	541.2
w/ DeepStack [10]	$53.2_{-3.3}$	$54.0_{-10.5}$	$54.6_{-9.5}$	$41.0_{-6.5}$	$52.9_{-3.1}$	$57.1_{-4.6}$	$88.2_{-0.6}$	$46.2_{-2.2}$	$53.3_{-0.4}$	$490.5_{-50.7}$
w/ SLI [12]	$\mathbf{57.2}_{+0.7}$	$64.7_{+0.2}$	$63.6_{-0.5}$	$46.6_{-0.9}$	$55.1_{-0.9}$	$55.2_{-6.5}$	$89.0_{+0.2}$	$\mathbf{48.8}_{+0.4}$	$54.5_{+0.8}$	$534.7_{-6.5}$
w/ **CLI**	$56.7_{+0.2}$	$\mathbf{65.2}_{+0.7}$	$\mathbf{64.7}_{+0.6}$	$47.1_{-0.4}$	$\mathbf{56.7}_{+0.7}$	$61.1_{-0.6}$	$\mathbf{89.1}_{+0.3}$	$48.6_{+0.2}$	**53.7**	$542.9_{+1.7}$
LLaVA-OV-7B	77.5	78.5	82.5	69.5	**68.4**	68.0	88.6	58.5	59.4	650.9
w/ DeepStack [10]	$76.0_{-1.5}$	$63.8_{-14.7}$	$72.6_{-9.9}$	$62.2_{-7.3}$	$61.4_{-7.0}$	$70.3_{+2.3}$	$88.7_{+0.1}$	$58.3_{-0.2}$	$58.5_{-0.9}$	$611.8_{-39.1}$
w/ SLI [12]	$77.6_{+0.1}$	$77.3_{-1.2}$	$79.9_{-2.6}$	$67.6_{-1.9}$	$68.2_{-0.2}$	$68.5_{+0.5}$	$89.0_{+0.4}$	$58.4_{-0.1}$	$59.3_{-0.1}$	$645.8_{-5.1}$
w/ **CLI**	$\mathbf{77.9}_{+0.4}$	$\mathbf{78.7}_{+0.2}$	$\mathbf{82.8}_{+0.3}$	$\mathbf{70.5}_{+1.0}$	**68.4**	$\mathbf{74.5}_{+6.5}$	$88.9_{+0.3}$	$\mathbf{59.2}_{+0.7}$	$\mathbf{59.7}_{+0.3}$	$\mathbf{660.6}_{+9.7}$

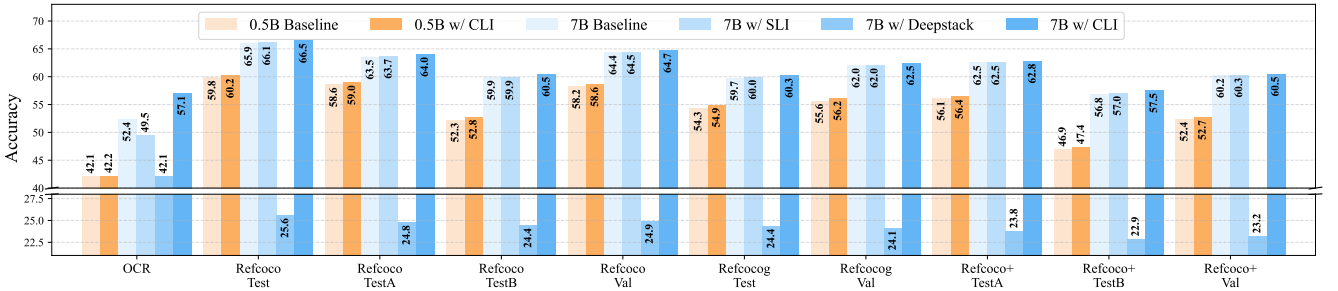

Figure 4. Performance gains from CLI on fine-grained visual reasoning. On both OCR and a comprehensive suite of visual grounding benchmarks (RefCOCO/+/g), CLI delivers consistent improvements for both the 0.5B and 7B models. This result demonstrates the framework's effectiveness in leveraging hierarchical visual features for tasks demanding high spatial and textural precision.

the LLM's shallowest layers, leaving the deeper, reasoning-intensive layers perceptually impoverished. In stark contrast, CLI's dynamic many-to-many architecture, governed by AGF, allows every designated LLM layer to query the entire visual hierarchy. This context-aware fusion enables a more sophisticated integration of visual evidence, leading to demonstrably superior performance.

Specifically, the benefits of CLI's architecture are evident across diverse task categories. For **fine-grained document understanding** on benchmarks like AI2D, ChartQA, DocVQA, and InfoVQA, CLI delivers cumulative gains of +1.1% and +1.9% over the Baseline Projector for the 0.5B and 7B models, respectively, by granting access to early-layer ViT features rich in essential textural and structural details. This strength extends to **complex multimodal reasoning**, where the impressive +6.5% gain on LLaVA-in-the-Wild with open-ended questions for the 7B model showcases how the AGF mechanism allows the LLM to dynamically synthesize information from the entire visual hierarchy—a capability static methods lack. Consistent gains

on other reasoning-heavy benchmarks like MME (+3.3% on 7B) and SEED-Bench (+1.1% on 0.5B) further confirm that rich, multi-level visual input is a critical component for high-level cognitive tasks. This enhancement further allows our CLI-enhanced models to compete with much larger systems. Notably, our LLaVA-OV-7B with CLI achieves a total score of 660.6, closing the performance gap to reach near-parity with the larger InternVL-2-8B model (660.9).

To further challenge the framework on tasks that depend critically on multi-level visual information, we evaluated it on a separate suite of fine-grained benchmarks: Optical Character Recognition (OCR) and visual grounding (as shown in Fig. 4). These tasks act as a stress-test for vision-language fusion, as they require the model to resolve fine character strokes (for OCR) or synthesize high-level semantic context with precise low-level localization (for visual grounding). Here, CLI's superiority is unambiguous. Its ability to tap into early-layer ViT features for high-fidelity detail proves decisive, yielding a remarkable **4.7%** improvement for the 7B model on OCR. Similarly,

Table 2. Main results on benchmarks for perception, multidisciplinary reasoning, and integrated capabilities. We compare our CLI-enhanced models against their baselines and alternative fusion methods on nine challenging benchmarks. The results demonstrate that CLI provides a consistent performance lift across different model architectures and sizes, confirming its effectiveness for tasks requiring complex reasoning and integrated visual understanding.

Model	MathVerse	MathVista	MMBench	MME	MMStar	MMMU	MMVet	SeedBench	ScienceQA	Sum
	mini-vision	testmini	en-dev	test	test	val	test	image	test	
VILA-13B [46]	26.4	33.7	57.9	45.2	32.8	31.5	31.2	66.5	71.0	396.2
IXC-2.5-7B [44]	13.03	60.4	66.1	90.3	14.8	33.1	46.3	47.1	22.0	380.1
InternVL-2-8B [45]	31.2	63.0	81.7	93.0	58.7	48.5	53.6	76.1	97.0	602.8
InternVL-2-26B [45]	27.3	61.1	81.6	94.9	60.4	47.5	53.1	76.7	97.5	600.1
LLaVA-OV-0.5B	17.7	36.3	45.8	63.2	38.5	30.7	28.0	65.6	65.2	391.0
w/ DeepStack [10]	17.8$_{-3.8}$	32.5$_{-3.8}$	**51.2**$_{+5.4}$	59.8$_{-3.4}$	38.5	**31.6**$_{+0.9}$	23.1$_{-4.9}$	62.9$_{-2.7}$	63.5$_{-1.7}$	380.9$_{-10.1}$
w/ SLI [12]	18.0$_{+0.3}$	**37.9**$_{+1.6}$	47.3$_{+1.5}$	61.1$_{-2.1}$	**42.6**$_{+4.1}$	30.2$_{-0.5}$	26.1$_{-1.9}$	65.9$_{+0.3}$	64.6$_{-0.6}$	393.7$_{+2.7}$
w/ **CLI**	**18.3**$_{+0.6}$	37.1$_{+0.8}$	48.3$_{+2.5}$	**63.3**$_{+0.1}$	39.3$_{+0.8}$	30.1$_{-0.6}$	27.0$_{-1.0}$	**66.7**$_{+1.1}$	**65.5**$_{+0.3}$	**395.6**$_{+4.6}$
LLaVA-OV-7B	**28.8**	55.4	79.2	85.1	54.1	47.0	**44.1**	76.1	**86.4**	556.2
w/ DeepStack [10]	27.0$_{-1.8}$	55.5$_{+0.1}$	78.1$_{-1.1}$	84.1$_{-1.0}$	50.8$_{-3.3}$	45.6$_{-1.4}$	40.3$_{-3.8}$	74.3$_{-1.8}$	83.6$_{-2.8}$	539.3$_{-16.9}$
w/ SLI [12]	25.9$_{-2.9}$	**57.8**$_{+2.4}$	**79.6**$_{+0.4}$	84.4$_{-0.7}$	55.8$_{+1.7}$	44.7$_{-2.3}$	40.6$_{-3.5}$	**76.5**$_{+0.4}$	85.8$_{-0.6}$	551.1$_{-5.1}$
w/ **CLI**	27.1$_{-1.7}$	55.8$_{+0.4}$	78.9$_{-0.3}$	**88.4**$_{+3.3}$	**56.5**$_{+2.4}$	**47.6**$_{+0.6}$	43.8$_{-0.3}$	75.7$_{-0.4}$	85.6$_{-0.8}$	**559.4**$_{+3.2}$

Table 3. To validate the architecture-agnostic nature of our method, we integrated CLI into the LLaVA-1.5 architecture. The CLI-enhanced model demonstrates consistent and broad performance gains across a wide range of tasks, from document understanding and real-world chat (top) to complex, multidisciplinary reasoning (bottom), confirming the robustness and general applicability of our framework.

Model	AI2D	ChartQA	DocVQA	InfoVQA	RealWorldQA	LLaVA-W	POPE	OK-VQA	GQA	Partial Sum
LLaVA-1.5-7B	66.3	38.9	32.2	26.8	54.5	62.9	87.0	41.8	57.6	468.0
w/ **CLI**	65.7$_{-0.6}$	39.6$_{+0.7}$	32.4$_{+0.2}$	26.3$_{-0.5}$	54.6$_{+0.1}$	65.9$_{+3.0}$	86.4$_{-0.6}$	47.0$_{+5.2}$	57.6	475.5$_{+7.5}$

Model	MathVerse	MathVista	MMBench	MME	MMStar	MMMU	MMVet	SeedBench	ScienceQA	Partial Sum
LLaVA-1.5-7B	17.5	34.4	64.3	79.9	37.2	34.5	31.2	61.9	72.9	433.8
w/ **CLI**	18.3$_{+0.8}$	35.6$_{+1.2}$	66.3$_{+2.0}$	79.4$_{-0.5}$	38.5$_{+1.3}$	35.7$_{+1.2}$	34.5$_{+3.3}$	61.9	72.2$_{-0.7}$	442.4$_{+8.6}$

it excels at grounding by allowing the LLM to dynamically draw on both deep ViT layers for context and shallow layers for spatial detail, leading to robust gains across **all nine** grounding benchmarks. This stands in stark contrast to the inconsistent results of competing methods as shown in Fig. 4, confirming that a dynamic, many-to-many architecture can reliably satisfy these complex visual demands.

In addition, to validate its generalizability, we ported CLI to the LLaVA-1.5 architecture, which uses a different LLM, vision encoder, and pre-training pipeline. As reported in Tab. 3, CLI delivers comprehensive performance improvements to this architecture as well. The gains on LLaVA-1.5 are even more pronounced than on LLaVA-OV (+7.5 and +8.6 partial sum improvements vs. +9.7 and +3.2). This suggests a deeper advantage of our framework: CLI can act as a compensatory mechanism, mitigating pre-existing weaknesses in a base model's original visual-language alignment. By forging a richer, more dynamic connection, CLI establishes a more robust multimodal foundation, highlighting its broad utility as a plug-and-play enhancement. (A comparison with DeepStack and SLI can be found in Appendix D.)

4.3. Ablation Studies

To dissect and validate our CLI framework, we conduct a series of ablation studies on LLaVA-OneVision-0.5B, analyzing component contributions and the injection strategy. For efficiency, these experiments use a 50% subset of the instruction tuning data, a point identified as a strong performance-to-cost trade-off in our scalability analysis (see Appendix E.1). The key findings on component roles and injection density are presented below, with more details on all ablations available in Appendix E.

Dissecting the Contributions of CLI Components. A component-wise ablation (Tab. 4) reveals the critical, synergistic roles of Adaptive Multi-Projection (AMP) and Adaptive Gating Fusion (AGF). Injecting multi-level features using only AMP provides marginal gains (367.89 vs. 366.72 baseline), confirming that simply flooding the LLM with unfiltered information is ineffective. In stark contrast, incorporating the AGF gating module alone yields a significant performance uplift (370.60), decisively validating our core hypothesis: the ability to dynamically select visual information is the most critical factor for successful fusion.

Table 4. Component-wise ablation study of the CLI framework on LLaVA-OV-0.5B. We incrementally add the AMP and the AGF module to the baseline. The results highlight the critical role of the gating mechanism and the synergy between both components.

Variant	AI2D	ChartQA	DocVQA	InfoVQA	MathVerse	MathVista	MMBench	MME	MMMU	Sum	Para
	test	test	val/test	val/test	mini-vision	testmini	en-dev	test	val		
Baseline	48.87	55.88	58.87	42.21	16.71	29.40	28.52	56.38	29.88	366.72	100.00%
w/ AMP	49.13	55.76	59.19	42.75	17.04	29.60	28.26	56.28	29.88	367.89	102.25%
w/ AGF	48.67	56.60	59.47	42.48	17.01	29.10	30.58	56.47	30.22	370.60	102.12%
w/ AMP + AGF	48.64	55.40	59.32	42.52	17.85	30.00	30.41	56.71	30.66	371.51	104.37%
w/ Full AMP	49.38	56.12	59.27	42.38	17.13	28.50	29.12	56.07	29.77	367.74	107.95%
w/ Full AMP + AGF	**51.30**	**62.72**	**60.76**	**44.71**	**18.06**	**33.30**	**45.79**	**58.49**	**31.88**	**407.01**	110.07%

Figure 5. Qualitative comparison of CLI on the LLaVA-OV-7B model across diverse benchmarks. Outputs from Baseline Projector are shown in red, while outputs from CLI are in green. The examples demonstrate that by integrating multi-level visual information, our model achieves more accurate perception and reasoning across various tasks, including MM-Star, LLaVA-in-the-Wild, and OCR-Bench.

The fine-tuned CLI framework, combining both modules, achieves further gains (371.51), demonstrating that AMP harmonizes the hierarchical features, providing a cleaner input for AGF to effectively gate. While a fully fine-tuned projector paired with AGF yields the highest absolute score (407.01), our LoRA-based AMP provides a much more compelling balance of performance and parameter efficiency (104.37% vs. 110.07% total params), justifying its use in our framework.

Impact of Injection Density. We next ablate the injection strategy to validate our many-to-many design (see Fig. 7 in Appendix E). Comparing various injection densities, we find that a single-point injection consistently underperforms, reaffirming that it creates an insurmountable information bottleneck. Conversely, a high-density strategy—injecting features frequently at multiple layers—achieves the best overall performance, powerfully validating our principle that on-demand access to the full visual hierarchy is essential. Intriguingly, a medium-density configuration underperforms a sparser one, suggesting a trade-off where intermittent updates may introduce disruptive cognitive overhead without the benefit of the near-continuous context provided by a high-density approach.

4.4. Visualizations

To offer insight into both the practical benefits and internal dynamics of our framework, we present qualitative and mechanistic visualizations. The qualitative examples in Fig. 5 highlight CLI's superior performance across diverse tasks. In complex compositional reasoning (MM-Star), fine-grained recognition (LLaVA-in-the-Wild), and challenging OCR, our model demonstrates more nuanced and accurate perception than the baseline. For instance, it correctly identifies a mangosteen where the baseline sees a durian, and reads the entire number '**3420**' where the baseline outputs a fragment, showcasing an ability to integrate both fine-grained details and global context.

The mechanism enabling this is revealed by visualizing the learned gating weights (Fig. 1(bottom)). The heatmap uncovers a complex, non-parallel "criss-crossed" information flow, providing compelling evidence for our many-to-many fusion thesis. It demonstrates an evolving demand for visual information throughout the LLM's decoding process: shallow decoder layers query early vision layers to ground basic concepts, while deeper layers tasked with complex reasoning learn to query the entire visual hierarchy. This allows them to simultaneously "zoom in" on fine details (crucial for OCR) and "zoom out" for global context (vital for reasoning). Together, these visualizations confirm that granting the LLM dynamic, on-demand access to the full visual hierarchy is essential for sophisticated multimodal understanding and validates the efficacy of CLI's design.

5. Conclusion

This paper introduces CLI, a framework that resolves the information bottleneck in VLMs by creating a dynamic "many-to-many" bridge between vision and language hierarchies. By granting the LLM on-demand access to all visual layers, CLI achieves significant performance gains across 18 diverse benchmarks. Our work validates that dynamic, selective fusion is critical for sophisticated reasoning, establishing CLI as a lightweight and scalable paradigm for deeper multimodal understanding.

8

6. Acknowledgments

References

[1] Jean-Baptiste Alayrac, Jeff Donahue, Pauline Luc, Antoine Miech, Iain Barr, Yana Hasson, Karel Lenc, Arthur Mensch, Katherine Millican, Malcolm Reynolds, Roman Ring, Eliza Rutherford, Serkan Cabi, Tengda Han, Zhitao Gong, Sina Samangooei, Marianne Monteiro, Jacob L. Menick, Sebastian Borgeaud, Andy Brock, Aida Nematzadeh, Sahand Sharifzadeh, Mikolaj Binkowski, Ricardo Barreira, Oriol Vinyals, Andrew Zisserman, and Karén Simonyan. Flamingo: a visual language model for few-shot learning. In Advances in Neural Information Processing Systems 35: Annual Conference on Neural Information Processing Systems 2022, NeurIPS 2022, New Orleans, LA, USA, November 28 - December 9, 2022, 2022. 1, 2

[2] Junnan Li, Dongxu Li, Silvio Savarese, and Steven C. H. Hoi. BLIP-2: bootstrapping language-image pre-training with frozen image encoders and large language models. In Andreas Krause, Emma Brunskill, Kyunghyun Cho, Barbara Engelhardt, Sivan Sabato, and Jonathan Scarlett, editors, International Conference on Machine Learning, ICML 2023, 23-29 July 2023, Honolulu, Hawaii, USA, volume 202 of Proceedings of Machine Learning Research, pages 19730–19742. PMLR, 2023. 2

[3] Haotian Liu, Chunyuan Li, Qingyang Wu, and Yong Jae Lee. Visual instruction tuning. In Advances in Neural Information Processing Systems 36: Annual Conference on Neural Information Processing Systems 2023, NeurIPS 2023, New Orleans, LA, USA, December 10 - 16, 2023, 2023. 2

[4] Haotian Liu, Chunyuan Li, Yuheng Li, and Yong Jae Lee. Improved baselines with visual instruction tuning. In IEEE/CVF Conference on Computer Vision and Pattern Recognition, CVPR 2024, Seattle, WA, USA, June 16-22, 2024, pages 26286–26296. IEEE, 2024. 1, 2, 5, 13, 16

[5] Alec Radford, Jong Wook Kim, Chris Hallacy, Aditya Ramesh, Gabriel Goh, Sandhini Agarwal, Girish Sastry, Amanda Askell, Pamela Mishkin, Jack Clark, Gretchen Krueger, and Ilya Sutskever. Learning transferable visual models from natural language supervision. In Proceedings of the 38th International Conference on Machine Learning, ICML 2021, 18-24 July 2021, Virtual Event, volume 139 of Proceedings of Machine Learning Research, pages 8748–8763. PMLR, 2021. 1, 5, 13

[6] Xiaohua Zhai, Basil Mustafa, Alexander Kolesnikov, and Lucas Beyer. Sigmoid loss for language image pre-training. In IEEE/CVF International Conference on Computer Vision, ICCV 2023, Paris, France, October 1-6, 2023, pages 11941–11952. IEEE, 2023. 1, 5, 13

[7] Giulio Starace, Konstantinos Papakostas, Rochelle Choenni, Apostolos Panagiotopoulos, Matteo Rosati, Alina Leidinger, and Ekaterina Shutova. Probing llms for joint encoding of linguistic categories. In Findings of the Association for Computational Linguistics: EMNLP 2023, Singapore, December 6-10, 2023, pages 7158–7179. Association for Computational Linguistics, 2023. 1, 2

[8] Xinyuan Song, Keyu Wang, Pengxiang Li, Lu Yin, and Shi-

wei Liu. Demystifying the roles of LLM layers in retrieval, knowledge, and reasoning. CoRR, abs/2510.02091, 2025. 2

[9] Shir Amir, Yossi Gandelsman, Shai Bagon, and Tali Dekel. Deep vit features as dense visual descriptors. CoRR, abs/2112.05814, 2021. 1, 2

[10] Lingchen Meng, Jianwei Yang, Rui Tian, Xiyang Dai, Zuxuan Wu, Jianfeng Gao, and Yu-Gang Jiang. Deep-stack: Deeply stacking visual tokens is surprisingly simple and effective for lmms. In Advances in Neural Information Processing Systems 38: Annual Conference on Neural Information Processing Systems 2024, NeurIPS 2024, Vancouver, BC, Canada, December 10 - 15, 2024, 2024. 2, 3, 5, 6, 7, 17

[11] Kaibing Chen, Dong Shen, Hanwen Zhong, Huasong Zhong, Kui Xia, Di Xu, Wei Yuan, Yifei Hu, Bin Wen, Tianke Zhang, Changyi Liu, Dewen Fan, Huihui Xiao, Jiahong Wu, Fan Yang, Size Li, and Di Zhang. EVLM: an efficient vision-language model for visual understanding. CoRR, abs/2407.14177, 2024. 2, 3

[12] Qwen Team. Qwen3-vl. https://github.com/QwenLM/Qwen3-VL, 2025. 2, 3, 5, 6, 7, 17

[13] Edward J. Hu, Yelong Shen, Phillip Wallis, Zeyuan Allen-Zhu, Yuanzhi Li, Shean Wang, Lu Wang, and Weizhu Chen. Lora: Low-rank adaptation of large language models. In The Tenth International Conference on Learning Representations, ICLR 2022, Virtual Event, April 25-29, 2022. OpenReview.net, 2022. 2

[14] Tom B. Brown, Benjamin Mann, Nick Ryder, Melanie Subbiah, Jared Kaplan, Prafulla Dhariwal, Arvind Neelakantan, Pranav Shyam, Girish Sastry, Amanda Askell, Sandhini Agarwal, Ariel Herbert-Voss, Gretchen Krueger, Tom Henighan, Rewon Child, Aditya Ramesh, Daniel M. Ziegler, Jeffrey Wu, Clemens Winter, Christopher Hesse, Mark Chen, Eric Sigler, Mateusz Litwin, Scott Gray, Benjamin Chess, Jack Clark, Christopher Berner, Sam McCandlish, Alec Radford, Ilya Sutskever, and Dario Amodei. Language models are few-shot learners. In Advances in Neural Information Processing Systems 33: Annual Conference on Neural Information Processing Systems 2020, NeurIPS 2020, December 6-12, 2020, virtual, 2020. 2

[15] Hugo Touvron, Thibaut Lavril, Gautier Izacard, Xavier Martinet, Marie-Anne Lachaux, Timothée Lacroix, Baptiste Rozière, Naman Goyal, Eric Hambro, Faisal Azhar, Aurélien Rodriguez, Armand Joulin, Edouard Grave, and Guillaume Lample. Llama: Open and efficient foundation language models. CoRR, abs/2302.13971, 2023. 2

[16] Wenliang Dai, Junnan Li, Dongxu Li, Anthony Meng Huat Tiong, Junqi Zhao, Weisheng Wang, Boyang Li, Pascale Fung, and Steven C. H. Hoi. Instructblip: Towards general-purpose vision-language models with instruction tuning. In Advances in Neural Information Processing Systems 36: Annual Conference on Neural Information Processing Systems 2023, NeurIPS 2023, New Orleans, LA, USA, December 10 - 16, 2023, 2023. 3

[17] Jun Chen, Deyao Zhu, Xiaoqian Shen, Xiang Li, Zechun Liu, Pengchuan Zhang, Raghuraman Krishnamoorthi, Vikas Chandra, Yunyang Xiong, and Mohamed Elhoseiny. Minigpt-v2: large language model as a unified interface for vision-language multi-task learning. CoRR, abs/2310.09478, 2023. 3

[18] Deyao Zhu, Jun Chen, Xiaoqian Shen, Xiang Li, and Mohamed Elhoseiny. Minigpt-4: Enhancing vision-language understanding with advanced large language models. In The Twelfth International Conference on Learning Representations, ICLR 2024, Vienna, Austria, May 7-11, 2024. OpenReview.net, 2024. 3

[19] Jinze Bai, Shuai Bai, Shusheng Yang, Shijie Wang, Sinan Tan, Peng Wang, Junyang Lin, Chang Zhou, and Jingren Zhou. Qwen-vl: A frontier large vision-language model with versatile abilities. CoRR, abs/2308.12966, 2023. 3

[20] Zhe Chen, Weiyun Wang, Yue Cao, Yangzhou Liu, Zhangwei Gao, Erfei Cui, Jinguo Zhu, Shenglong Ye, Hao Tian, Zhaoyang Liu, Lixin Gu, Xuehui Wang, Qingyun Li, Yimin Ren, Zixuan Chen, Jiapeng Luo, Jiahao Wang, Tan Jiang, Bo Wang, Conghui He, Botian Shi, Xingcheng Zhang, Han Lv, Yi Wang, Wenqi Shao, Pei Chu, Zhongying Tu, Tong He, Zhiyong Wu, Huipeng Deng, Jiaye Ge, Kai Chen, Min Dou, Lewei Lu, Xizhou Zhu, Tong Lu, Dahua Lin, Yu Qiao, Jifeng Dai, and Wenhai Wang. Expanding performance boundaries of open-source multimodal models with model, data, and test-time scaling. CoRR, abs/2412.05271, 2024. 3

[21] Zheng Liu, Mengjie Liu, Jingzhou Chen, Jingwei Xu, Bin Cui, Conghui He, and Wentao Zhang. FUSION: fully integration of vision-language representations for deep cross-modal understanding. CoRR, abs/2504.09925, 2025. 3

[22] Jiabo Ye, Haiyang Xu, Haowei Liu, Anwen Hu, Ming Yan, Qi Qian, Ji Zhang, Fei Huang, and Jingren Zhou. mplug-owl3: Towards long image-sequence understanding in multi-modal large language models. In The Thirteenth International Conference on Learning Representations, ICLR 2025, Singapore, April 24-28, 2025. OpenReview.net, 2025. 3

[23] Bo Li, Yuanhan Zhang, Dong Guo, Renrui Zhang, Feng Li, Hao Zhang, Kaichen Zhang, Peiyuan Zhang, Yanwei Li, Ziwei Liu, and Chunyuan Li. Llava-onevision: Easy visual task transfer. Trans. Mach. Learn. Res., 2025, 2025. 5, 13, 14

[24] An Yang, Baosong Yang, Binyuan Hui, Bo Zheng, Bowen Yu, Chang Zhou, Chengpeng Li, Chengyuan Li, Dayiheng Liu, Fei Huang, Guanting Dong, Haoran Wei, Huan Lin, Jialong Tang, Jialin Wang, Jian Yang, Jianhong Tu, Jianwei Zhang, Jianxin Ma, Jianxin Yang, Jin Xu, Jingren Zhou, Jinze Bai, Jinzheng He, Junyang Lin, Kai Dang, Keming Lu, Keqin Chen, Kexin Yang, Mei Li, Mingfeng Xue, Na Ni, Pei Zhang, Peng Wang, Ru Peng, Rui Men, Ruize Gao, Runji Lin, Shijie Wang, Shuai Bai, Sinan Tan, Tianhang Zhu, Tianhao Li, Tianyu Liu, Wenbin Ge, Xiaodong Deng, Xiaohuan Zhou, Xingzhang Ren, Xinyu Zhang, Xipin Wei, Xuancheng Ren, Xuejing Liu, Yang Fan, Yang Yao, Yichang Zhang, Yu Wan, Yunfei Chu, Yuqiong Liu, Zeyu Cui, Zhenru Zhang, Zhifang Guo, and Zhihao Fan. Qwen2 technical report. CoRR, abs/2407.10671, 2024. 5, 13

[25] Wei-Lin Chiang, Zhuohan Li, Zi Lin, Ying Sheng, Zhanghao Wu, Hao Zhang, Lianmin Zheng, Siyuan Zhuang, Yonghao Zhuang, Joseph E. Gonzalez, Ion Stoica, and Eric P. Xing. Vicuna: An open-source chatbot impressing gpt-4 with 90%* chatgpt quality, March 2023. 5, 13

10

[26] Kaichen Zhang, Bo Li, Peiyuan Zhang, Fanyi Pu, Joshua Adrian Cahyono, Kairui Hu, Shuai Liu, Yuanhan Zhang, Jingkang Yang, Chunyuan Li, and Ziwei Liu. Lmms-eval: Reality check on the evaluation of large multimodal models. In Findings of the Association for Computational Linguistics: NAACL 2025, Albuquerque, New Mexico, USA, April 29 - May 4, 2025, pages 881–916. Association for Computational Linguistics, 2025. 5, 15

[27] Aniruddha Kembhavi, Mike Salvato, Eric Kolve, Min Joon Seo, Hannaneh Hajishirzi, and Ali Farhadi. A diagram is worth a dozen images. In Computer Vision - ECCV 2016 - 14th European Conference, Amsterdam, The Netherlands, October 11-14, 2016, Proceedings, Part IV, volume 9908 of Lecture Notes in Computer Science, pages 235–251. Springer, 2016. 5, 15

[28] Ahmed Masry, Do Xuan Long, Jia Qing Tan, Shafiq R. Joty, and Enamul Hoque. Chartqa: A benchmark for question answering about charts with visual and logical reasoning. In Findings of the Association for Computational Linguistics: ACL 2022, Dublin, Ireland, May 22-27, 2022, pages 2263–2279. Association for Computational Linguistics, 2022. 5, 15

[29] Minesh Mathew, Dimosthenis Karatzas, and C. V. Jawahar. Docvqa: A dataset for VQA on document images. In IEEE Winter Conference on Applications of Computer Vision, WACV 2021, Waikoloa, HI, USA, January 3-8, 2021, pages 2199–2208. IEEE, 2021. 5, 15

[30] Minesh Mathew, Viraj Bagal, Rubèn Tito, Dimosthenis Karatzas, Ernest Valveny, and C. V. Jawahar. Infographicvqa. In IEEE/CVF Winter Conference on Applications of Computer Vision, WACV 2022, Waikoloa, HI, USA, January 3-8, 2022, pages 2582–2591. IEEE, 2022. 5, 15

[31] Shukang Yin, Chaoyou Fu, Sirui Zhao, Ke Li, Xing Sun, Tong Xu, and Enhong Chen. A survey on multimodal large language models. CoRR, abs/2306.13549, 2023. 5, 15

[32] Yuan Liu, Haodong Duan, Yuanhan Zhang, Bo Li, Songyang Zhang, Wangbo Zhao, Yike Yuan, Jiaqi Wang, Conghui He, Ziwei Liu, Kai Chen, and Dahua Lin. Mmbench: Is your multi-modal model an all-around player? In Computer Vision - ECCV 2024 - 18th European Conference, Milan, Italy, September 29-October 4, 2024, Proceedings, Part VI, volume 15064 of Lecture Notes in Computer Science, pages 216–233. Springer, 2024. 5, 15

[33] Weihao Yu, Zhengyuan Yang, Linjie Li, Jianfeng Wang, Kevin Lin, Zicheng Liu, Xinchao Wang, and Lijuan Wang. Mm-vet: Evaluating large multimodal models for integrated capabilities. In Forty-first International Conference on Machine Learning, ICML 2024, Vienna, Austria, July 21-27, 2024. OpenReview.net, 2024. 5, 15

[34] Renrui Zhang, Dongzhi Jiang, Yichi Zhang, Haokun Lin, Ziyu Guo, Pengshuo Qiu, Aojun Zhou, Pan Lu, Kai-Wei Chang, Yu Qiao, Peng Gao, and Hongsheng Li. MATH-VERSE: does your multi-modal LLM truly see the diagrams in visual math problems? In Computer Vision - ECCV 2024 - 18th European Conference, Milan, Italy, September 29-October 4, 2024, Proceedings, Part VIII, volume 15066 of Lecture Notes in Computer Science, pages 169–186. Springer, 2024. 5, 15

[35] Pan Lu, Hritik Bansal, Tony Xia, Jiacheng Liu, Chunyuan Li, Hannaneh Hajishirzi, Hao Cheng, Kai-Wei Chang, Michel Galley, and Jianfeng Gao. Mathvista: Evaluating math reasoning in visual contexts with gpt-4v, bard, and other large multimodal models. CoRR, abs/2310.02255, 2023. 5, 15

[36] Xiang Yue, Yuansheng Ni, Tianyu Zheng, Kai Zhang, Ruoqi Liu, Ge Zhang, Samuel Stevens, Dongfu Jiang, Weiming Ren, Yuxuan Sun, Cong Wei, Botao Yu, Ruibin Yuan, Renliang Sun, Ming Yin, Boyuan Zheng, Zhenzhu Yang, Yibo Liu, Wenhao Huang, Huan Sun, Yu Su, and Wenhu Chen. MMMU: A massive multi-discipline multimodal understanding and reasoning benchmark for expert AGI. In IEEE/CVF Conference on Computer Vision and Pattern Recognition, CVPR 2024, Seattle, WA, USA, June 16-22, 2024, pages 9556–9567. IEEE, 2024. 5, 15

[37] Drew A. Hudson and Christopher D. Manning. GQA: A new dataset for real-world visual reasoning and compositional question answering. In IEEE Conference on Computer Vision and Pattern Recognition, CVPR 2019, Long Beach, CA, USA, June 16-20, 2019, pages 6700–6709. Computer Vision Foundation / IEEE, 2019. 5, 15

[38] Kenneth Marino, Mohammad Rastegari, Ali Farhadi, and Roozbeh Mottaghi. OK-VQA: A visual question answering benchmark requiring external knowledge. In IEEE Conference on Computer Vision and Pattern Recognition, CVPR 2019, Long Beach, CA, USA, June 16-20, 2019, pages 3195–3204. Computer Vision Foundation / IEEE, 2019. 5, 15

[39] Pan Lu, Swaroop Mishra, Tanglin Xia, Liang Qiu, Kai-Wei Chang, Song-Chun Zhu, Oyvind Tafjord, Peter Clark, and Ashwin Kalyan. Learn to explain: Multimodal reasoning via thought chains for science question answering. In Advances in Neural Information Processing Systems 35: Annual Conference on Neural Information Processing Systems 2022, NeurIPS 2022, New Orleans, LA, USA, November 28 - December 9, 2022, 2022. 5, 15

[40] Jie Ying, Zihong Chen, Zhefan Wang, Wanli Jiang, Chenyang Wang, Zhonghang Yuan, Haoyang Su, Huanjun Kong, Fan Yang, and Nanqing Dong. Seedbench: A multi-task benchmark for evaluating large language models in seed science. In Proceedings of the 63rd Annual Meeting of the Association for Computational Linguistics (Volume 1: Long Papers), ACL 2025, Vienna, Austria, July 27 - August 1, 2025, pages 31395–31449. Association for Computational Linguistics, 2025. 5, 15

[41] Lin Chen, Jinsong Li, Xiaoyi Dong, Pan Zhang, Yuhang Zang, Zehui Chen, Haodong Duan, Jiaqi Wang, Yu Qiao, Dahua Lin, and Feng Zhao. Are we on the right way for evaluating large vision-language models? In Advances in Neural Information Processing Systems 38: Annual Conference on Neural Information Processing Systems 2024, NeurIPS 2024, Vancouver, BC, Canada, December 10 - 15, 2024, 2024. 5, 16

[42] Yifan Li, Yifan Du, Kun Zhou, Jinpeng Wang, Wayne Xin Zhao, and Ji-Rong Wen. Evaluating object hallucination in large vision-language models. In Proceedings of the 2023 Conference on Empirical Methods in Natural Language Processing, EMNLP 2023, Singapore, December

6-10, 2023, pages 292–305. Association for Computational Linguistics, 2023. 5, 16

[43] X.AI Corp. Grok-1.5 vision preview: Connecting the digital and physical worlds with our first multimodal model. https://x.ai/blog/grok-1.5v, 2024. 5, 16

[44] Pan Zhang, Xiaoyi Dong, Yuhang Zang, Yuhang Cao, Rui Qian, Lin Chen, Qipeng Guo, Haodong Duan, Bin Wang, Linke Ouyang, Songyang Zhang, Wenwei Zhang, Yining Li, Yang Gao, Peng Sun, Xinyue Zhang, Wei Li, Jingwen Li, Wenhai Wang, Hang Yan, Conghui He, Xingcheng Zhang, Kai Chen, Jifeng Dai, Yu Qiao, Dahua Lin, and Jiaqi Wang. Internlm-xcomposer-2.5: A versatile large vision language model supporting long-contextual input and output. CoRR, abs/2407.03320, 2024. 5, 6, 7

[45] Zhe Chen, Jiannan Wu, Wenhai Wang, Weijie Su, Guo Chen, Sen Xing, Muyan Zhong, Qinglong Zhang, Xizhou Zhu, Lewei Lu, Bin Li, Ping Luo, Tong Lu, Yu Qiao, and Jifeng Dai. Internvl: Scaling up vision foundation models and aligning for generic visual-linguistic tasks. CoRR, abs/2312.14238, 2023. 5, 6, 7

[46] Ji Lin, Hongxu Yin, Wei Ping, Pavlo Molchanov, Mohammad Shoeybi, and Song Han. VILA: on pre-training for visual language models. In IEEE/CVF Conference on Computer Vision and Pattern Recognition, CVPR 2024, Seattle, WA, USA, June 16-22, 2024, pages 26679–26689. IEEE, 2024. 5, 6, 7

From One-to-One to Many-to-Many: Dynamic Cross-Layer Injection for Deep Vision-Language Fusion

Supplementary Material

A. Model Configuration

This section provides a detailed description of the model configurations and training protocols for the baseline models used in our experiments, namely LLaVA-OneVision and LLaVA-1.5. The settings are adopted from their original papers [4, 23] to ensure a fair and reproducible comparison.

A.1. LLaVA-OneVision

Architecture. Our methodology adopts the LLaVA-OneVision architecture [23] as its foundational structure. To investigate scalability, our experiments are conducted using its publicly available 0.5B and 7B parameter variants. This established VLM framework comprises three core components that enable its cross-modal capabilities.

First, the language model (LLM) backbone consists of the Qwen2 series models, specifically Qwen2-0.5B and Qwen2-7B [24]. The LLaVA-OneVision framework leverages these models for their robust language understanding and complex reasoning capabilities, which are essential for interpreting and acting upon user instructions. Second, visual understanding is handled by a pre-trained SigLIP vision encoder, Siglip-so400m-patch14-384 [6]. The selection of this encoder provides the baseline with a powerful and generalizable foundation for feature extraction, stemming from its extensive pre-training on diverse web-scale data. Finally, a projector module, implemented as a two-layer Multilayer Perceptron (MLP), serves to bridge the two modalities. Its function within the architecture is to map the visual features from the SigLIP encoder's output space into the LLM's input embedding space, thereby allowing the language model to process visual and textual information in a unified manner.

CLI Configuration Details. For both the 0.5B and 7B variants of our CLI-enhanced LLaVA-OneVision models, we implemented a consistent high-density, many-to-many injection strategy. We extract hierarchical visual features from the 28-layer SigLIP vision encoder by sampling every **fourth** layer. These multi-level features are then injected into the LLM decoder at **corresponding intervals**. Specifically, for the LLaVA-OV-0.5B model, which comprises a 24-layer Qwen2-0.5B backbone, injections occur at every fourth layer. A similar strategy with a stride of four is applied to the 28-layer Qwen2-7B backbone of the LLaVA-OV-7B model.

To harmonize the features from diverse vision layers, our **Adaptive Multi-Projection (AMP)** module augments the pre-trained projector with layer-specific Low-Rank Adaptation (LoRA). For these adaptations, we configure the LoRA parameters with a rank of 128 and an alpha of 128. At each designated injection point within the LLM, an **Adaptive Gating Fusion (AGF)** module governs the selective integration of these hierarchical visual features. The AGF mechanism first distills information from both modalities independently. For the visual input, a learnable query vector (q_v) attends to the projected visual features (acting as key and value) via multi-head self-attention. Concurrently, another learnable query (q_h) probes the LLM's current hidden states to produce a contextual summary. The resulting context vectors from both attention modules are concatenated and processed by a gate controller, implemented as a linear layer. Finally, a Sigmoid activation function is applied to this fused representation to produce a dynamic weight, which determines the degree to which the new visual information updates the LLM's hidden state.

Training Strategy. Our training diverges from the full curriculum of the original LLaVA-OneVision. We start from the official checkpoint released after its "Stage-1.5: High-Quality Knowledge Learning" phase. Our training consists solely of the subsequent **Single-Image Fine-tuning** stage. This stage involves fine-tuning the entire model on an approximately 1.4 million sample dataset. This dataset was curated by randomly sampling from the full 3.2M single-image instruction data pool described in the original paper. The detailed composition of our sampled dataset is provided in Appendix B. To select the optimal checkpoint and prevent overfitting, the training was conducted for up to three epoch, governed by an early stopping mechanism based on performance on a held-out validation set. The specific hyperparameters for our fine-tuning process are detailed in Tab. 5.

A.2. LLaVA-1.5

Architecture. In parallel with our primary experiments, we also benchmark our approach against the widely-used LLaVA-1.5 framework [4], specifically leveraging its 7B parameter version to ensure a fair comparison. This established architecture also integrates three distinct components to facilitate its cross-modal understanding. First, the core of its reasoning and generative capabilities is the Vicuna-7B (v1.5) model [25], which serves as the language backbone. Second, for visual perception, the framework employs a pre-trained CLIP vision encoder (CLIP-ViT-L-336px) [5].

Table 5. Fine-tuning configuration for our LLaVA-OneVision models. This table details the settings for the single-image fine-tuning stage we performed.

Parameter	Value
Vision	
Resolution	$384 \times \{\{1 \times 1\}, \ldots, \{6 \times 6\}\}$
Max #Tokens	729×10
Data	
Dataset	Single-Image Instruction Data
#Samples	$\sim$1.4M (Sampled)
Model	
Trainable	Full Model
Parameters (0.5B)	0.8B
Parameters (7B)	8.0B
Training Hyperparameters	
Batch Size (0.5B)	256
Batch Size (7B)	256
LR: Vision Encoder	2×10^{-6}
LR: Projector & LLM	1×10^{-5}
Epochs	Up to 3 (with Early Stopping)

This module is configured to process input images at a resolution of 336x336 pixels to extract high-level visual features. Finally, a two-layer Multilayer Perceptron (MLP), featuring a GELU activation function, acts as the projector. This crucial component connects the vision and language modalities by mapping the output features from the CLIP encoder into the input embedding space of the Vicuna language model.

CLI Implementation on LLaVA-1.5. To validate the architecture-agnostic nature of our framework, we integrated CLI into the LLaVA-1.5-7B model. This architecture features a different set of core components: a 32-layer Vicuna-7B model as the LLM backbone and a 24-layer CLIP-ViT-L-336px as the vision encoder. To maintain consistency with our primary experiments, we adopted the same high-density injection strategy. Specifically, we extract hierarchical visual features by sampling every **fourth** layer from the 24-layer CLIP encoder. These multi-level features are then injected into the 32-layer Vicuna decoder, also at a stride of every **fourth layer**. The core mechanisms of our CLI framework, including the LoRA-based **Adaptive Multi-Projection (AMP)** and the query-based **Adaptive Gating Fusion (AGF)** modules, remain identical to the configuration used for the LLaVA-OneVision models, ensuring a fair and direct comparison of the framework's generalizability.

Training Strategy. Our LLaVA-1.5 experiments start from the official pre-trained checkpoint, which has completed Stage-1 (Vision-Language Alignment). Our work thus consists exclusively of the second stage: **Visual Instruction Tuning (Fine-tuning)**. To ensure a fair comparison between model architectures, we utilized the identical training dataset and procedure as in our LLaVA-OneVision experiments. Specifically, the entire model was fine-tuned on the same $\sim$1.4 million sampled single-image instruction dataset. The hyperparameters for our fine-tuning process are listed in Tab. 6.

Table 6. Fine-tuning configuration for our LLaVA-1.5 model. This table details the settings for the visual instruction tuning stage we performed.

Hyperparameter	Value
Batch Size	256
Learning Rate (LR)	2×10^{-5}
LR Schedule	Cosine Decay
LR Warmup Ratio	0.03
Weight Decay	0
Epochs	1
Optimizer	AdamW

B. Instruction Tuning Dataset Details

Our fine-tuning process utilizes a meticulously curated instruction-following dataset of approximately 1.4 million samples. This dataset is a sampled subset of the comprehensive 3.2 million single-image data pool introduced in the LLaVA-OneVision paper [23]. The goal of our curation was to create a high-quality, balanced mixture that covers a wide range of visual tasks while remaining computationally efficient for our experiments.

Data Composition. Following the categorization of LLaVA-OneVision, our dataset is composed of five principal categories to ensure a diverse skill set for the fine-tuned models:

- **General QA and Conversation:** This is the largest category, designed to enhance the model's core visual dialogue and question-answering capabilities. It includes data from sources like ShareGPT4V/4o, Vision FLAN, and the general-purpose instruction sets from Cambrian and ALLaVA.
- **Math and Reasoning:** To bolster the model's logical and spatial reasoning abilities, we incorporated a significant portion of math-related visual question-answering data. Key sources include Geo170K, MathQA, and various datasets from the MathV360K collection.

- **Document, Chart, and Screen Understanding:** This category focuses on fine-grained perception of structured information. We sampled from datasets such as UReader, ChartQA, AI2D, and InfographicVQA.
- **General OCR:** To improve text recognition in natural scenes, we included data from sources like TextCaps and IAM.
- **Language:** To maintain and enhance the underlying language capabilities of the LLM, we included a substantial amount of high-quality, text-only instruction data from the Magpie-Pro collection.

Sampling Strategy. Instead of using the entire 3.2M sample pool, we employed a curated sampling strategy to construct our final dataset. As detailed in Tab. 7, this involved taking all samples from some smaller, high-quality sources (e.g., GEOS, Diagram Image2Text) while applying percentage-based sampling to larger datasets. This approach allowed us to tailor the contribution of each data source, creating a balanced and effective training mixture. All data was formatted according to the LLaVA prompting strategy to ensure compatibility and avoid instructional conflicts.

C. Evaluation Benchmarks

To ensure a standardized and reproducible comparison, we evaluate all models across a comprehensive suite of single-image benchmarks using the open-source LMMs-Eval framework [26]. These benchmarks are grouped into three primary categories to assess a wide range of capabilities, from fine-grained perception to complex, real-world reasoning. All evaluations are conducted in a zero-shot setting unless otherwise specified.

Evaluation Metrics. Our evaluation primarily relies on the standard metrics implemented within the LMMs-Eval framework. For most benchmarks involving definite answers (e.g., multiple-choice or single-word VQA), we report standard **Accuracy**. For text-centric VQA tasks like DocVQA, we use **Average Normalized Levenshtein Similarity (ANLS)** to robustly measure performance against potential OCR inaccuracies. For open-ended conversational benchmarks such as LLaVA-in-the-Wild, we employ **GPT-assisted evaluation**, where GPT-4 serves as a judge to score model responses.

We employ specific aggregation methods for two benchmarks to derive a single, comparable score:
- For the **MME** benchmark, we report a unified success rate. This is calculated by summing the raw *cognition_score* and *perception_score* and then dividing by the total number of samples across both categories.

- For the **MathVerse** benchmark, the final score is the average accuracy across its three sub-tasks: *vision_intensive*, *vision_only*, and *vision_dominant*.

Chart, Diagram, and Document Understanding. This category of benchmarks tests the models' ability to perform fine-grained perception and reasoning on structured visual information, which often involves understanding text, layouts, and data visualizations.
- **AI2D** [27]: A benchmark for question answering on science diagrams, requiring parsing of diagrammatic elements and text.
- **ChartQA** [28]: A question-answering dataset focused on charts, which demands both visual perception and logical reasoning over the data presented.
- **DocVQA** [29]: A dataset for visual question answering on document images, testing the model's ability to read and comprehend text in complex layouts.
- **InfoVQA** [30]: A benchmark for VQA on infographics, requiring the model to synthesize information from a mix of text, charts, and images.

Perception and Multidisciplinary Reasoning. This group of benchmarks evaluates the models' core visual perception skills and their ability to integrate this perception with world knowledge for complex reasoning across multiple disciplines.
- **MME** [31]: A comprehensive benchmark designed to evaluate both the perception and cognition capabilities of multimodal models.
- **MMBench** [32]: A multi-discipline benchmark that assesses models on a wide range of skills through multiple-choice questions.
- **MMVet** [33]: Evaluates large multimodal models for their integrated capabilities across six core vision-language domains.
- **MathVerse** [34]: A benchmark focused on visual math problems, specifically testing the ability to understand diagrams and figures in a mathematical context.
- **MathVista** [35]: A comprehensive benchmark for evaluating mathematical reasoning in diverse visual contexts.
- **MMMU** [36]: A massive multi-discipline benchmark that assesses models on college-level problems requiring expert-level understanding and reasoning.
- **GQA** [37]: A dataset for real-world visual reasoning and compositional question answering.
- **OK-VQA** [38]: A visual question answering benchmark where questions require external knowledge beyond what is present in the image.
- **ScienceQA** [39]: A multimodal dataset for science question answering, involving text, diagrams, and formulas.
- **SEED-Bench** [40]: A multi-task benchmark for evaluating the generative comprehension of LMMs.

Table 7. Detailed composition of the ∼1.4M instruction tuning dataset used in our experiments.

General (1,011,544 samples)			
Dataset	**# Samples**	**Dataset**	**# Samples**
ALLaVA Instruct	20,994	ScienceQA	498
AOKVQA	1,654	ShareGPT4o	57,284
Cambrian (filtered)	83,125	ShareGPT4V	90,985
Hateful Memes	850	TallyQA	4,934
IconQA	1,130	Vision FLAN (filtered)	184,173
Image Textualization	9,958	Visual7W	1,437
LLaVA-NeXT Base	369,294	VisualWebInstruct	263,583
LLaVAR	1,979	VisText	997
LRV Normal (filtered)	1,049	VizWiz	661
PMC-VQA	360	VQARAD	31
		VSR	216
		WebSight	1,000

Math/Reasoning (71,321 samples)			
Dataset	**# Samples**	**Dataset**	**# Samples**
CLEVR-Math	528	MAVIS (Metagen & Rule)	18,734
FigureQA	1,759	MathQA	29,827
GEOS	498	MapQA	4,265
Geo170K (Align & QA)	12,808	Super-CLEVR	865
GeoMVerse	930	TabMWP	3,382
GeoQA+	1,717	TQA	1,366
Geometry3K	3,064	UniGeo	1,195
InterGPS	128		

Doc/Chart/Screen (77,349 samples)			
Dataset	**# Samples**	**Dataset**	**# Samples**
AI2D	8,534	MultiHierTT (Cauldron)	762
Chart2Text	2,696	RoBUT SQA	851
ChartQA	1,826	RoBUT WikiSQL	7,499
Diagram Image2Text	295	Screen2Words	1,573
HiTab	250	UReader (Cap, IE, KG, QA)	39,927
Infographic VQA	6,588	VisualMRC	303
LRV Chart	1,776		

General OCR (6,472 samples)		Language (179,993 samples)	
Dataset	**# Samples**	**Dataset**	**# Samples**
IAM	566	Magpie Pro (L3 MT)	59,998
Rendered Text	1,000	Magpie Pro (L3 ST)	59,998
ST-VQA	1,725	Magpie Pro (Qwen2 ST)	59,997
TextCaps	2,195		
TextOCR (GPT4V)	2,511		

- **MM-Star** [41]: A benchmark designed with challenging examples to test the limits of advanced VLMs.
- **POPE** [42]: A benchmark specifically designed to evaluate object hallucination in large vision-language models by testing their polling-based object presence evaluation.

Real-world Understanding and Visual Chat. This category assesses the practical utility of models as general-purpose visual assistants in open-ended, real-world scenarios.

- **RealWorldQA** [43]: A benchmark containing questions about real-world images, often requiring common-sense reasoning and detailed observation.
- **LLaVA-in-the-Wild** [4]: A set of challenging, open-ended visual conversation prompts designed to evaluate the practical chat capabilities of LMMs in unconstrained scenarios.

Table 8. To validate the architecture-agnostic nature of our method, we integrated CLI into the LLaVA-1.5 architecture. The CLI-enhanced model demonstrates consistent and broad performance gains across a wide range of tasks, from document understanding and real-world chat (top) to complex, multidisciplinary reasoning (bottom), confirming the robustness and general applicability of our framework.

Model	AI2D	ChartQA	DocVQA	InfoVQA	RealWorldQA	LLaVA-W	POPE	OK-VQA	GQA	Partial Sum
LLaVA-1.5-7B	**66.3**	38.9	32.2/-	**26.8**/-	54.5	62.9	**87.0**	41.8	**57.6**	468.0
w/ DeepStack [10]	65.4$_{-0.9}$	**41.4**$_{+2.5}$	**33.1**$_{+0.9}$/-	26.2$_{-0.6}$/-	48.7$_{-5.8}$	47.7$_{-15.2}$	86.7$_{-0.3}$	43.3$_{+1.5}$	57.0$_{-0.6}$	449.5$_{-18.5}$
w/ SLI [12]	64.8$_{-1.5}$	38.0$_{-0.9}$	30.4$_{-1.8}$/-	24.7$_{-2.1}$/-	52.9$_{-1.6}$	56.1$_{-6.8}$	86.3$_{-0.7}$	**50.6**$_{+8.8}$	57.0$_{-0.6}$	460.8$_{-7.2}$
w/ CLI	65.7$_{-0.6}$	39.6$_{+0.7}$	32.4$_{+0.2}$/-	26.3$_{-0.5}$/-	**54.6**$_{+0.1}$	**65.9**$_{+3.0}$	86.4$_{-0.6}$	47.0$_{+5.2}$	**57.6**	**475.5**$_{+7.5}$

Model	MathVerse	MathVista	MMBench	MME	MMStar	MMMU	MMVet	SeedBench	ScienceQA	Partial Sum
LLaVA-1.5-7B	17.5	34.4	64.3	**79.9**	37.2	34.5	31.2	**61.9**	**72.9**	433.8
w/ DeepStack [10]	12.3$_{-5.2}$	34.8$_{+0.4}$	63.2$_{-1.1}$	76.0$_{-3.9}$	37.5$_{+0.3}$	**36.5**$_{+2.0}$	**34.5**$_{+3.3}$	61.0$_{-0.9}$	70.5$_{-2.4}$	426.3$_{-7.5}$
w/ SLI [12]	17.7$_{+0.2}$	33.7$_{-0.7}$	62.6$_{-1.7}$	76.6$_{-3.3}$	35.3$_{-1.9}$	35.3$_{+0.8}$	30.6$_{-0.6}$	51.6$_{-10.3}$	72.8$_{-0.1}$	416.2$_{-17.6}$
w/ CLI	**18.3**$_{+0.8}$	**35.6**$_{+1.2}$	**66.3**$_{+2.0}$	79.4$_{-0.5}$	**38.5**$_{+1.3}$	35.7$_{+1.2}$	**34.5**$_{+3.3}$	**61.9**	72.2$_{-0.7}$	**442.4**$_{+8.6}$

D. Deepstack and SLI in LLaVA-1.5

To validate the architecture-agnostic nature of our framework and conduct a rigorous comparison against alternative deep fusion strategies, we integrated **CLI**, **DeepStack**, and **SLI** into the LLaVA-1.5-7B architecture. The results, detailed in Tab. 8, not only confirm the general applicability of CLI but also highlight the fundamental limitations of non-adaptive fusion methods.

The brute-force, one-to-many injection of visual features of DeepStack proves highly detrimental, leading to a substantial performance degradation, with partial sum scores dropping by 18.5 and 7.5 points. This negative impact was particularly pronounced on conversational benchmarks like LLaVA-W (-15.2%), supporting the hypothesis that unfiltered, non-selective feature injection disrupts the LLM's learned representations and generative coherence.

Similarly, the statically-wired, one-to-one approach of SLI resulted in a significant performance collapse. This method, which creates a rigid mapping between initial vision encoder layers and shallow LLM decoder layers, was particularly damaging for complex reasoning tasks. The partial sum score on multidisciplinary reasoning benchmarks plummeted by a catastrophic 28.6 points, with severe losses on benchmarks like MMMU (-10.2%) and SEED-Bench (-10.3%). This failure demonstrates that confining multi-level visual information to the LLM's shallowest layers perceptually impoverishes the deeper, reasoning-intensive layers, leaving them unable to access the visual details required for sophisticated problem-solving.

In stark contrast, our **CLI** framework delivered consistent and significant performance improvements, boosting the partial sum scores by +7.5% and +8.6%. The dynamic, context-aware selection enabled by **CLI's** AGF module allows the LLM to selectively integrate the most relevant visual features, thereby enriching its understanding without disrupting its internal representations. This experiment thus validates **CLI** as a robust and superior paradigm for deep vision-language fusion whose benefits generalize across diverse model architectures.

E. More Details on Ablation Studies

To rigorously validate the design of our CLI framework, we conduct a series of ablation studies on LLaVA-OV-0.5B. These experiments are designed to analyze the impact of data scale, dissect the individual contributions of our key components, and determine the optimal injection strategy.

E.1. Impact of Instruction Data Volume

To investigate the data efficiency and scalability of our CLI framework, we first analyze its performance when trained on varying subsets of the instruction tuning data (20%, 50%, and 80%). As shown in Fig. 6, the results reveal a nuanced relationship between data volume, task type, yielding five key insights. First, in the absence of any instruction tuning (the 0% case), the model's performance is negligible, confirming the critical role of this training phase for instruction-following. Second, performance gains are most significant in the low-data regime (from 0% to 50%), after which the rate of improvement begins to plateau, indicating diminishing returns. Third, despite these diminishing returns, the CLI framework consistently achieves superior peak performance. At the 100% data point, CLI outperforms or matches the baseline on seven of the eight benchmarks, demonstrating that our architecture is not only more data-efficient but also attains a higher final performance level. Fourth, the amount of data required for CLI to surpass the baseline is highly task-dependent. For **fine-grained perception tasks** (e.g., DocVQA, InfoVQA) that necessitate precise OCR and layout understanding, CLI requires more data to realize its full advantage; its performance curve typically intersects and then surpasses the baseline's around the 50% data mark, suggesting that learning to leverage multi-level details for high-fidelity perception is a data-intensive process. Fifth, in contrast, for **reasoning-intensive tasks** (e.g., MM-Star, MathVerse), the architectural advantages of CLI are apparent even at low data volumes. The frame-
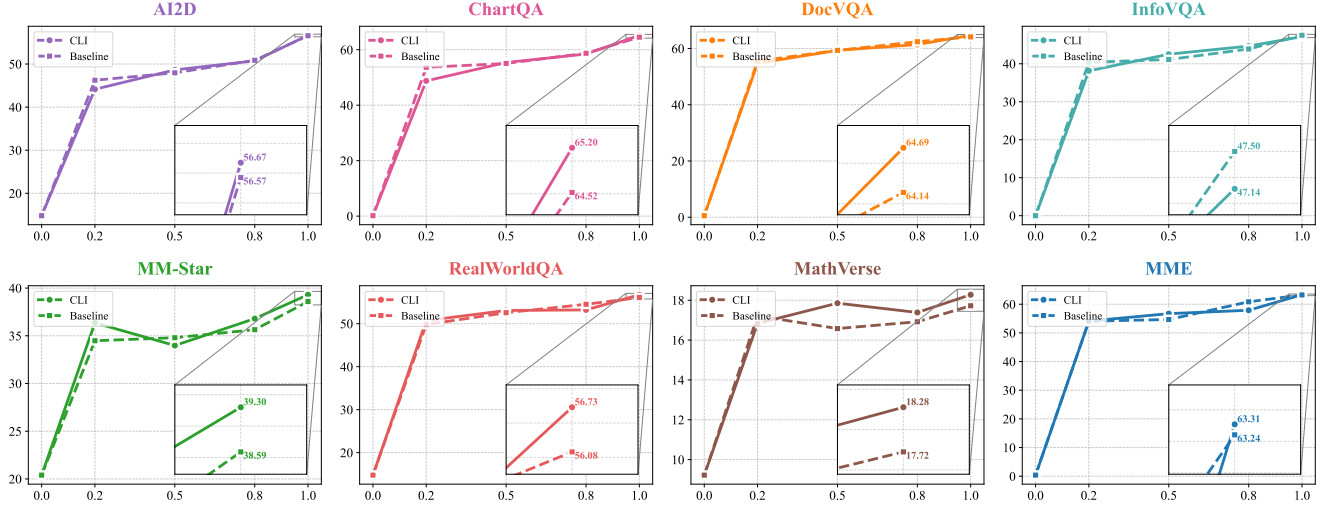
Figure 6. Ablation study on the effect of training data volume. Performance of our proposed framework (CLI) and the baseline model is evaluated on eight benchmarks using varying percentages of the instruction tuning dataset. Our framework consistently improves performance and effectively leverages larger instruction sets, confirming its robustness at different data scales.

work establishes a significant performance lead over the baseline with as little as 20% of the training data, indicating that its dynamic integration of global context with local details provides a more data-efficient strategy for complex reasoning, enabling the model to acquire effective problem-solving heuristics more rapidly. Based on this analysis, we identify the 50% data subset as an efficient trade-off point for conducting further, more computationally intensive ablations.

E.2. Dissecting the Contributions of CLI Components

The efficacy of our framework is predicated upon two synergistic modules: the Adaptive Multi-level Projector (AMP) for harmonizing hierarchical features and the Attentional Gating Funnel (AGF) for their selective injection. To isolate their individual and combined impacts, we conducted a component-wise ablation study, with results presented in Tab. 4. We first test the effect of injecting multi-level features without a gating mechanism. Variants *w/* AMP show only marginal gains over the baseline. This is a critical finding: merely flooding the LLM with hierarchical visual information is ineffective and risks causing information overload. Without a mechanism to filter for relevance, the model cannot effectively utilize the richer data stream. Further, in stark contrast, a variant that incorporates only the AGF module yields a significant performance uplift. This result decisively validates our core hypothesis: the most crucial element for effective hierarchical fusion is empowering the LLM to act as an active observer, dynamically selecting visual information based on its real-time decoding context. The ability to selectively gate information is more impor-

tant than the richness of the information itself. Finally, we observe the synergy between our modules. When AMP is added to the gating mechanism, performance improves further. This confirms that adapting the projector to the distinct statistical distributions of different vision layers provides the AGF with a cleaner, more harmonized set of features, making its selection process more effective.

To further evaluate the efficiency of our proposed AMP, we conduct experiments where a dedicated projector is fully fine-tuned for each selected layer. As indicated in Tab. 4, this full fine-tuning approach, despite its increased parameter count (107.95% vs 102.25%), results in performance degradation compared to our standard AMP (367.74 vs 367.89). We hypothesize this degradation stems from two key risks of full fine-tuning: catastrophic forgetting, by overwriting the projector's valuable pre-trained knowledge, and overfitting on the limited dataset due to the model's expanded parameter space. However, when this fully fine-tuned projector is augmented with our AGF, it achieves the highest performance. A potential explanation is that while full fine-tuning unlocks maximum representational capacity, only a mechanism like AGF can effectively harness it by selecting salient features and mitigating noise. Finally, given the superior balance between performance and parameter efficiency, we adopt the parameter-efficient LoRA-based AMP in our final framework, as it provides a compelling and scalable alternative to full fine-tuning.

E.3. Impact of Injection Density

Further, we conduct an ablation study by varying the density of cross-layer injection points to probe the effectiveness of our dynamic "many-to-many" architecture. The results,
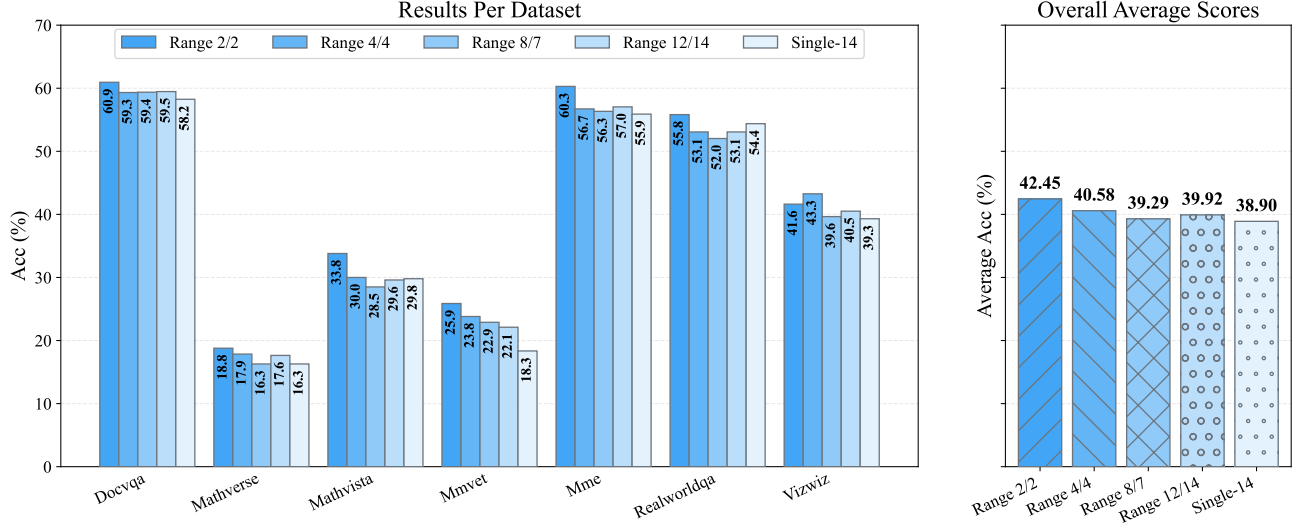
Figure 7. Ablation study on the density of cross-layer injection points. The performance of different injection strategies—from high-density ('2/2') to a single-layer baseline ('Single-14')—is evaluated across several benchmarks. The high-density configuration achieves the best overall performance, validating our many-to-many design.

as shown in Fig. 7, are highly revealing: the 'Single-14' baseline consistently underperforms, reaffirming that a single static feature map creates an insurmountable information bottleneck. Conversely, the high-density '2/2' strategy achieves the best overall performance, powerfully validating our principle that frequent access to the full visual hierarchy allows the AGF module to effectively navigate the dense information stream. Intriguingly, the study also uncovers a crucial trade-off between information gain and cognitive overhead, as the medium-density '8/7' configuration underperforms the sparser '12/14' strategy. We hypothesize that the '8/7' setting introduces disruptive cognitive overhead without the benefit of near-continuous context, whereas the '12/14' strategy offers a more "economical" and stable, albeit less powerful, update schedule.

F. Qualitative Analysis: Strengths and Limitations

To provide an intuitive understanding of our CLI framework's performance, we present a series of qualitative case studies in Fig. 8.

Complex Visual Reasoning and Instruction Following. The bottom-left panel provides the most compelling evidence of CLI's advanced reasoning capabilities. The prompt asks for the "biggest word written in white". The baseline model identifies "EMBRACE". This indicates a failure to grasp the holistic message of the image. In stark contrast, our CLI model correctly identifies "love." This

success demonstrates that CLI, by integrating global context with local details, enables the LLM to achieve a deeper semantic understanding of the scene. This showcases a leap from simple perception to sophisticated, non-literal multimodal reasoning.

Robustness in Challenging OCR and Hallucination Reduction. The top row illustrates performance on OCR tasks of varying difficulty. For the clear, standard font in the top-left example ("Otter Bitter"), both models perform competently, establishing a baseline. The top-right case, however, presents a highly stylized, artistic font that is challenging for both architectures. Here, the baseline model fails catastrophically, hallucinating the unrelated word "god" due to the weak and ambiguous visual signal. Our CLI model, while also unable to decipher the entire word, correctly identifies the initial, more legible part, "getty." This demonstrates a critical advantage of CLI: improved visual grounding. By providing richer, multi-level visual evidence, CLI anchors the LLM's output to the actual image content, effectively suppressing the tendency to invent information and thus reducing catastrophic hallucinations.

Reliable Common-Sense Reasoning. The bottom-right example probes the models' alignment with common-sense world knowledge. Our CLI model provides the standard, expected answer ("Yes," cats typically hunt mice). The baseline's response ("No") is unpredictable and counterintuitive. While one could argue for a nuanced interpreta-

Figure 8. Qualitative comparison of CLI and the baseline on diverse visual reasoning tasks.

tion, this erratic behavior, when viewed alongside its other failures, points to a less reliable reasoning process. CLI's response, in this context, demonstrates more stable and predictable alignment with general knowledge.

In summary, these qualitative examples illustrate that CLI not only enhances fine-grained perception but, more importantly, enables the model to perform complex visual-linguistic reasoning, improves its robustness against hallucination in ambiguous scenarios, and ensures more reliable alignment with common-sense knowledge.